RSC Advances

PAPER

View Article Online
View Journal | View Issue

Cite this: *RSC Adv.*, 2025, **15**, 37579

Electrochemical sensor based on molecularly imprinted polymer and voltammetric electronic tongue technology: an efficient strategy for sensitive detection of tobramycin residues

Makhtar War,[a] Fatih Şen, *[b] Ebru Halvaci,[b] Benachir Bouchikhi[a] and Nezha El Bari*[a]

Tobramycin (TOB) is an aminoglycoside antibiotic widely used to treat chronic lung infections and other bacterial diseases. However, TOB residues may persist in food products derived from animals treated with antibiotics, posing a risk of promoting antibiotic resistance in consumers. This highlights the urgent need for sensitive and selective methods to detect TOB residues in food. In this study, both an electrochemical sensor based on a conductive molecularly imprinted polymer (MIP) and a voltammetric electronic tongue (VET) system were developed for the detection of TOB. The MIP sensor was fabricated by electropolymerizing polyaniline onto a screen-printed gold electrode (Au-SPE), with the sensitivity further enhanced by the incorporation of silver nanoparticles. Surface morphology characterization of the modified electrodes was carried out using scanning electron microscopy (SEM), and Fourier transform infrared spectroscopy (FTIR). Cyclic voltammetry (CV), differential pulse voltammetry (DPV), and electrochemical impedance spectroscopy (EIS) were employed to characterize the sensors during both their fabrication and the TOB detection process. The sensors exhibited a detection limit of 1.9 pg mL^{-1} within a concentration range of 0.001–60 pg mL^{-1}. The MIP sensors were selective for TOB, and were successfully applied to the detection of TOB residues in various food samples, including chicken, beef, turkey, chicken eggs, and milk. The VET system combined with chemometric methods particularly demonstrated its effectiveness in detecting TOB in milk samples. Principal component analysis (PCA) and discriminant function analysis (DFA) confirmed the ability of the VET system to differentiate between TOB-contaminated and uncontaminated milk samples, with PCA explaining 96.94% of the variance. This study presents a significant advance in the electrochemical detection of antibiotics in food, demonstrating the potential of MIP-based sensors, VET system for practical applications in food safety monitoring, and public health analysis.

Received 4th June 2025
Accepted 8th September 2025

DOI: 10.1039/d5ra03963k

rsc.li/rsc-advances

1 Introduction

Antibiotic resistance has emerged as a critical global health crisis, posing a severe threat to public health worldwide. According to the Centers for Disease Control and Prevention (CDC), antibiotic-resistant infections account for approximately 2.8 million illnesses annually in the United States alone, while globally, these infections contribute to an estimated 10 million deaths each year.[1,2] Antibiotics such as tobramycin (TOB) have played a transformative role in modern medicine, providing effective treatment for a broad spectrum of infectious diseases in both humans and livestock.[3–5]

TOB is an aminoglycoside antibiotic consisting of two or more amino sugars linked *via* glycosidic bonds to a central aminocyclitol nucleus, specifically 2-deoxystreptamine.[6] It is biosynthesized through the fermentation of *Streptomyces tenebrarius* and is incorporated into pharmaceutical formulations such as TOBraDex® and TOBI®. TOB features five protonation equilibria (pK_a values ranging from 5.67 to 9.29), which contribute to its high aqueous solubility and broad-spectrum antibacterial activity.[7,8] Aminoglycosides are primarily employed against aerobic Gram-negative bacteria, with some efficacy against Gram-positive pathogens as well.[9]

Upon ingestion through the food chain, TOB is absorbed, metabolized by the liver, and ultimately excreted *via* the kidneys. However, its accumulation in the body can lead to adverse effects, including hepatotoxicity and nephrotoxicity, some of which may be irreversible.[10] Given these risks, accurate and sensitive detection of TOB residues is essential in clinical

[a]*Biosensors and Nanotechnology Group, Department of Biology, Faculty of Sciences, Moulay Ismail University, B.P. 11201, Zitoune, 50003, Meknes, Morocco. E-mail: nezhaelbari6@gmail.com; fatih.sen@dpu.edu.tr; Fax: +212 5 35 53 68 08; Tel: +212 6 61 35 84 32*

[b]*Department of Biochemistry, Kutahya Dumlupinar University, Kütahya, Turkey*

diagnostics, environmental assessments, and food safety monitoring.

To mitigate health risks associated with antibiotic residues, regulatory agencies such as the European Commission have established strict maximum residue limits (MRLs) for aminoglycosides in food products. Specifically, the MRL for TOB in milk has been set at 200 $\mu g \cdot kg^{-1}$.[8,11]

A comprehensive review of existing literature reveals several analytical techniques currently employed for the detection of TOB in food products. These include high-performance liquid chromatography (HPLC),[12] liquid chromatography–mass spectrometry (LC-MS),[13] capillary electrophoresis,[14] colorimetric methods,[15] and fluorescence spectroscopy.[16] While these methods offer high sensitivity and reproducibility for both qualitative and quantitative analyses, they are often constrained by significant drawbacks such as high operational costs, labor-intensive and time-consuming sample preparation, and the requirement for trained personnel.[17,18]

In contrast, electrochemical techniques have gained prominence due to their inherent advantages namely simplicity, rapid response, high sensitivity, energy efficiency, operational stability, and cost-effectiveness. These methods also allow for on-site analysis, making them ideal for field-based and real-time monitoring.[19,20]

Among emerging technologies, molecularly imprinted polymers (MIPs) have garnered significant attention for their high selectivity in target recognition. MIPs are engineered to possess specific binding sites complementary to the target molecule in shape, size, and functional groups.[21,22] Electropolymerization is commonly used to synthesize MIPs, offering precise control over film thickness and deposition rate by adjusting parameters such as applied voltage, number of cycles, and monomer-to-template ratios.[23] This fine-tuning capability makes MIP-based sensors highly adaptable for various analytical applications.

The incorporation of nanomaterials, such as silver nanoparticles (AgNPs), further enhances electrochemical sensor performance by facilitating rapid electron transfer and increasing the active surface area.[24] Additionally, screen-printed electrodes (SPEs), particularly those utilizing gold due to its chemical stability and conductivity, are widely adopted for the development of disposable, cost-effective MIP-based sensors.[25,26]

Given the critical need for effective TOB monitoring, recent studies have focused on advanced electrochemical sensors integrating nanomaterials and aptamers for enhanced performance. For instance, a "sandwich-type" aptamer-based sensor incorporating AgNPs and polydopamine nanospheres (PDANSs) achieved a detection limit of 1.41 pM and demonstrated excellent reproducibility in environmental samples.[27] Another approach utilized metal–organic frameworks (MOFs) to amplify the signal, achieving low nanomolar detection thresholds.[28] Further, a label-free electrochemical aptasensor on a glassy carbon electrode modified with nanocomposites reached a detection limit of 4.0 pM for antibiotics like sulfamethazine.[29]

Other innovative approaches include bimetallic cerium/copper oxides embedded in mesoporous carbon,[30] MnCo oxide nanohybrids for enhanced sensitivity in biological matrices,[27] and gold nanostructure-based aptamer platforms for improved surface area and conductivity.[31] Reviews by Mobed *et al.*[30] highlight the growing application of biosensors for pharmaceutical detection, while Garcia-Guzman *et al.*[32] introduced a microneedle-based electrochemical sensor for continuous antibiotic monitoring. Dual-antibiotic detection systems[33] and photoelectrochemical (PEC) sensors using SnO_2/Bi_2S_3 composites[34] have also been explored, further broadening the detection landscape.

In this study, we report the development of an electrochemical MIP sensor and an aptamer-based detection platform for TOB, optimized for food safety applications. The aptamer sensor achieved a linear detection range of 5–50 nM with a detection limit of 0.88 nM, indicating high sensitivity. While biological matrix interference remains a challenge, this work explores the application of multi-sensor systems combined with multivariate data analysis to improve selectivity and robustness. The rapid advancements in TOB detection technologies presented here contribute to the development of portable, sensitive, and specific sensors for environmental monitoring, food safety, and clinical applications, addressing a critical gap in current literature.[35–38]

The study also investigates a voltammetric electronic tongue (VET) system, which is an array of cross-sensitive electrochemical sensors designed to mimic the human gustatory system. These sensors generate complex signal patterns analyzed using pattern recognition and chemometric techniques such as principal component analysis (PCA), discriminant function analysis (DFA), support vector machines (SVMs), and receiver operating characteristic (ROC) analysis.[39] These tools enhance data interpretation, visualization, and TOB prediction accuracy.

Specifically, the electrochemical MIP sensor developed here was characterized using cyclic voltammetry (CV), differential pulse voltammetry (DPV), electrochemical impedance spectroscopy (EIS), scanning electron microscopy (SEM), and Fourier-transform infrared spectroscopy (FTIR). Its performance, measured in terms of sensitivity, detection limit, selectivity, and cross-reactivity, was benchmarked against prior technologies. The VET system was applied to TOB analysis in milk, utilizing multivariate models to classify and predict TOB levels effectively. Together, these innovations provide a robust platform for the detection of TOB in food matrices such as chicken, beef, turkey, eggs, and milk, contributing significantly to food safety monitoring and public health protection.

2 Experimentation

2.1 Reagents and solutions

All chemicals used in this study were of analytical grade and utilized without further purification. Aniline (99%) was obtained from the Faculty of Sciences and Technology, University Hassan II of Mohammedia (Morocco). Ammonium persulfate (APS), used as the oxidizing agent in the polymerization process, was sourced from Fluka (Germany).

For electrochemical characterization, potassium ferricyanide $[K_3Fe(CN)_6]$ and potassium ferrocyanide $[K_4Fe(CN)_6]$ were

both purchased from Fluka (Germany). Methanol (99.8%) and acetic acid (99.9%), used for extracting TOB from the molecularly imprinted polymer (MIP) matrix, were supplied by Riedel-de-Haën. Silver nitrate (99.8%) and trisodium citrate (99.5%), essential for the synthesis of silver nanoparticles (AgNPs), were obtained from Sigma-Aldrich (France).

A phosphate-buffered saline (PBS) solution (0.01 M, pH ~7.2) was used as the supporting electrolyte to maintain a stable, near-neutral environment during electrochemical measurements. All solutions and preparations were made using distilled water to ensure experimental consistency and reproducibility. The product samples, such as turkey, chicken, and beef, came from a local supermarket in Meknes (Morocco), KOUTOUBIA.

2.2 Apparatus

Electrochemical measurements were conducted using screen-printed gold electrodes (Au-SPEs) serving as transducers. Each Au-SPE included a gold working electrode (0.19 cm^2), a silver reference electrode, and a gold auxiliary electrode (0.54 cm^2). These electrodes were procured from Sigma-Aldrich (Spain). All electrochemical characterizations were performed using a PalmSens³ potentiostat (Netherlands), connected to a computer and operated *via* PS-Trace software. A junction box facilitated the interface between the Au-SPEs and the PalmSens3 system.[38]

During the fabrication of the TOB molecularly imprinted polymer (MIP) sensor, surface morphology and elemental composition of the electrodes were analyzed using scanning electron microscopy (SEM) and Fourier-transform infrared spectroscopy (FTIR). SEM imaging was conducted at Moulay Ismaïl University of Meknes using a JSM-IT500HR scanning electron microscope at a magnification of ×20 000 and an acceleration voltage of 15 kV. These images provided detailed insights into the surface features of the modified electrodes.

FTIR analysis was carried out using a Bruker Alpha II FTIR-ATR spectrometer (Meknes, Morocco). Spectra were recorded in the range of 500–4000 cm^{-1}, with a background spectrum collected prior to each measurement. This analysis was used to characterize the chemical structure of the polymeric films formed on the electrode surface.

2.3 Preparation of AgNPs

Silver nanoparticles (AgNPs) were synthesized *via* a chemical reduction method using trisodium citrate as the reducing agent. Specifically, 80 mg of silver nitrate ($AgNO_3$) was dissolved in 200 mL of distilled water and brought to a boil. Once the solution reached boiling point, 3 mL of a 1% (w/v) trisodium citrate solution ($C_6H_5O_7Na_3$) was added gradually, drop by drop, under continuous heating. The appearance of a pale-yellow color indicated the formation of silver nanoparticles.[40] The solution was then stirred until it cooled to room temperature (25 °C), resulting in a stable colloidal suspension of AgNPs.

The chemical reduction reaction is represented as follows:

$$4Ag^+ + C_6H_5O_7Na_3 + 2H_2O \rightarrow 4Ago + C_6H_5O_7H_3 + 3Na^+ + H^+ + O_2 \quad (1)$$

In this reaction, silver ions (Ag^+) are reduced to elemental silver (Ag^0) by citrate ions in an aqueous medium. Concurrently, the citrate is oxidized to citric acid ($C_6H_5O_7H_3$). The process also releases sodium ions (Na^+), hydrogen ions (H^+), and oxygen gas (O_2). This method provides a straightforward and reproducible route to synthesizing AgNPs, which play a critical role in enhancing the electrochemical performance of sensors through improved conductivity and electron transfer.

2.4 Preparation of polyaniline

Polyaniline (PANI) was synthesized *via* oxidative polymerization through a controlled, stepwise procedure. Initially, 7 mmol of aniline was dissolved in 20 mL of distilled water and stirred with a magnetic stir bar for 10 min. The solution was then cooled to a temperature range of 0–5 °C and maintained under these conditions for 30 min with continued stirring. In parallel, 7 mmol of ammonium persulfate (APS) was dissolved in 80 mL of freshly distilled water to prepare the oxidizing solution.

The APS solution was added in a single portion to the pre-cooled aniline solution. The resulting mixture was stirred continuously for 1 hour and kept at 0–5 °C for an extended polymerization period of 24 hours to ensure complete formation of the polymer.[41]

The final product, polyaniline (PANI), is a conductive polymer recognized for its excellent chemical stability, high electrical conductivity, and ease of synthesis. Its unique combination of electrical, optical, and electrochemical properties makes it highly applicable in various electrochemical devices, sensors, and energy storage systems.[42]

2.5 Preparation of the MIP and NIP-based sensors

The objective of this study was to develop a molecularly imprinted polymer (MIP) sensor capable of selectively detecting TOB in real food samples, as illustrated in Fig. 1. The physicochemical properties of TOB are summarized in Table 1.

To begin the sensor fabrication, bare gold screen-printed electrodes (Au-SPEs) were cleaned by thorough rinsing with distilled water, followed by sonication to remove surface impurities. A composite solution (designated as Solution S1) was prepared containing 1.25 mL of TOB, 5 mL of polyaniline (PANI), and 250 μL of silver nanoparticles (AgNPs). The monomer-to-template ratio was of 4.

A 50 μL aliquot of Solution S1 was then electropolymerized onto the Au-SPE surface using cyclic voltammetry (CV). The electropolymerization was conducted over a potential range of −0.4 V to +0.6 V, at a scan rate of 20 mV s^{-1} for 10 cycles. These optimized parameters were selected to ensure uniform deposition of the composite and to prevent aggregation of AgNPs, thereby promoting even distribution across the electrode surface. The incorporation of AgNPs was intended to enhance the sensor's electroactive surface area, improve electron transfer kinetics, and increase overall sensitivity.

During electropolymerization, the working electrode gradually formed a complex between the TOB molecules and the growing polymer matrix. Following polymerization, TOB was extracted from the polymer layer, creating selective recognition

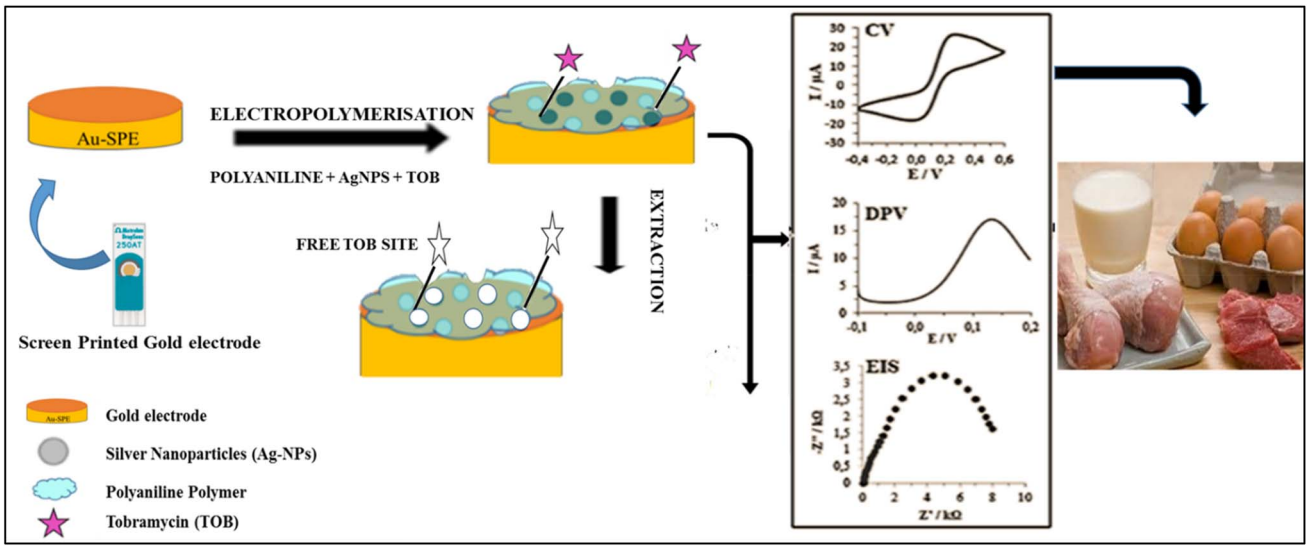

Fig. 1 Manufacturing process of the molecularly imprinted polymer sensor.

Table 1 Physico-chemical properties of tobramycin

Structure formula	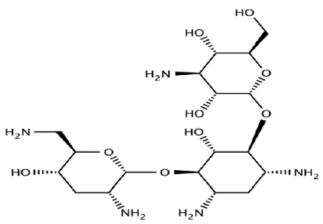
IUPAC nomenclature	*O*-3-Amino-3-deoxy-alpha-D-glucopyranosyl-(1-4)-*O*-(2,6-diamino-trideoxy-alpha-D ribohexpoyranosy l-(1-4))-2-deoxy-D-streptamine
Molecular formula	$C_{18}H_{37}N_5O_9$
Molecular weight	467.52 g mol^{-1}
Water solubility	Freely soluble in water
pK_{a1}	12.54 (strongest acid)
pK_{a1}	9.83 (strongest base)

sites. These are molecular cavities complementary in size, shape, and chemical functionality to TOB. After this step, the obtained device was washed with PBS (pH = 7.2) and dried for the retention process. These imprinted sites enable the sensor to selectively bind and detect TOB in subsequent analyses.

For control purposes, a non-imprinted polymer (NIP) sensor was also fabricated using an identical procedure, except without the inclusion of TOB in the polymerization mixture (designated as Solution S2). This allowed comparison between selective and non-selective responses and helped confirm the specificity of the MIP-based system.

2.6 Electrochemical parameters

Following immobilization of the MIP layer onto the Au-SPE surface, the sensor was characterized using a series of electrochemical techniques, including cyclic voltammetry (CV), electrochemical impedance spectroscopy (EIS), and differential pulse voltammetry (DPV). These analyses were conducted in a 0.01 M phosphate-buffered saline (PBS) solution at pH 7.2, using 5 mM ferricyanide/ferrocyanide ($[Fe(CN)_6]^{3-/4-}$) as the redox probe.

These techniques provided critical insights into the sensor's electrochemical behavior, including its binding efficiency, surface properties, and sensitivity toward TOB. CV was performed within a potential range of −0.4 V to +0.6 V at a scan rate of 20 mV s^{-1} to evaluate redox activity before and after TOB binding.

To complement the CV results and assess the interface properties of the sensor surface, EIS measurements were carried out under open circuit potential conditions. An AC voltage of 10 mV was applied over a frequency range of 0.1 Hz to 50 kHz, using a sampling density of 50 frequency points.

DPV was used to further evaluate TOB retention by the MIP sensor. Measurements were performed at a scan rate of 20 mV

s^{-1}, with the potential range maintained between −0.4 V and +0.6 V. All electrochemical experiments were conducted at room temperature (25 °C) to maintain consistency and reproducibility.

2.7 Synthetic detection of TOB

In accordance with European Union regulations, the maximum permissible limit for TOB is 12 μg mL^{-1} in serum[16] and 200 μg kg^{-1} in milk.[43–45] To facilitate sensor calibration and performance evaluation, a TOB stock solution was prepared at a concentration of 0.003 g mL^{-1}. This stock solution was serially diluted in phosphate-buffered saline (PBS, pH 7.2) to produce a range of working concentrations reflective of typical TOB levels in food matrices.

The final concentration series, labelled C1 through C7, was as follows:

C1: 0.001 pg mL^{-1}; C2: 0.008 pg mL^{-1}; C3: 0.05 pg mL^{-1}; C4: 0.3 pg mL^{-1}; C5: 2.0 pg mL^{-1}; C6: 9.9 pg mL^{-1}; C7: 60.0 pg mL^{-1}.

This range ensured comprehensive evaluation of the sensor's detection capabilities across trace-level to higher concentrations, consistent with regulatory and practical relevance in food safety monitoring.

2.8 Applications of MIP sensor for TOB detection in real samples

Milk, meat, and egg samples were procured from local markets in Meknes, Morocco, for experimental analysis. To prepare skimmed milk, 50 mL of raw milk was centrifuged at 10 000 rpm for 15 min at 4 °C to remove fat globules. Meat samples were finely chopped and ground to produce homogenized extracts, which were subsequently clarified by centrifugation under the same conditions to eliminate particulate matter.

Egg samples were stored at −20 °C prior to analysis. For sample preparation, 1.0 g of egg white was mixed with 10 mL of phosphate buffer (pH 7.2) and homogenized for 2 min. The homogenate was then centrifuged at 4500 rpm for 15 min, and the supernatant was collected for further analysis.

These prepared extracts were used in subsequent electrochemical testing to evaluate the sensor's performance, sensitivity, and selectivity across different biological matrices, thereby ensuring robustness and real-world applicability.[46,47,61]

2.9 VE-tongue experimental set-up

The experimental setup for voltammetric electronic tongue (VET) analysis of milk samples, illustrated in Fig. 2, utilized a conventional three-electrode electrochemical cell. The configuration consisted of an Ag/AgCl reference electrode, a platinum auxiliary electrode, and an array of five distinct working electrodes: copper (Cu), glassy carbon (GC), platinum (Pt), palladium (Pd), and gold (Au). Each working electrode was chosen for its specific electrochemical characteristics, enabling the system to capture a broad range of electrochemical signals.

The choice of electrodes in the VE-Tongue system for analysing TOB-containing samples is driven by the need for a sensitive, and robust electrochemical device capable of detecting this aminoglycoside antibiotic in complex matrices. TOB, with its amino and hydroxyl functional groups, is not highly electroactive but can interact with electrode surfaces *via* adsorption, complexation, or indirect reactions. The VE-Tongue system employs an Ag/AgCl reference electrode for stability, a platinum auxiliary electrode for robustness, and five working electrodes (glassy carbon, gold, palladium, copper, platinum). Noble electrodes ensure sensitive detection through adsorption, while non-noble electrodes enhance selectivity *via* chemical reactions.

This multi-electrode array allowed for comprehensive profiling of the milk matrix by generating diverse and complementary sensor responses. The configuration is particularly effective for analyzing complex biological samples such as milk,

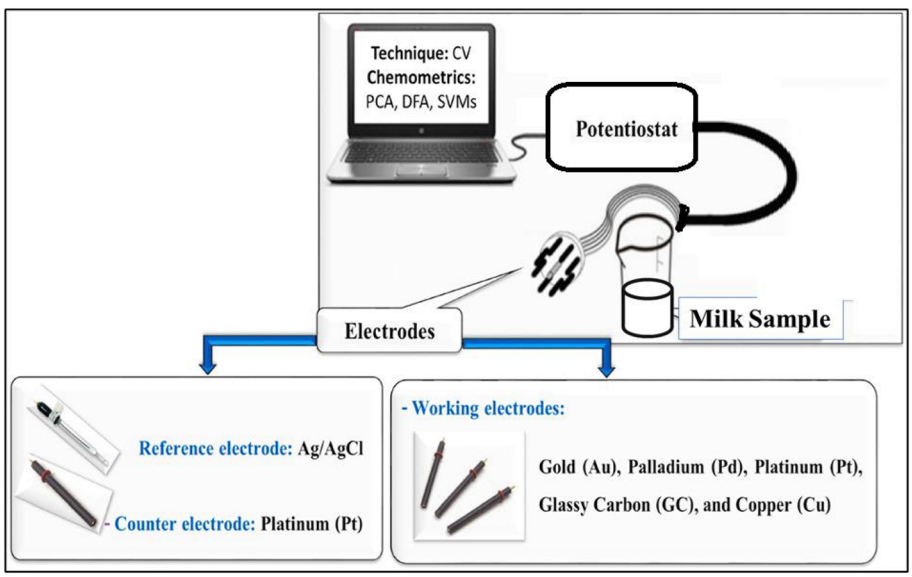

Fig. 2 Schematic representation of the voltammetric electronic tongue dedicated to the analysis of milk samples.

offering enhanced sensitivity and selectivity through sensor diversity. This platform supports robust multivariate analysis and pattern recognition, key components of the VET system's analytical capability.

2.10 Data analysis

A voltammetric electronic tongue (VET) was employed for the qualitative analysis of eight milk samples spiked with varying concentrations of TOB, ranging from 0 to 60 pg mL^{-1}. The electrochemical cell was equipped with five working electrodes, along with a reference and auxiliary electrode. Cyclic voltammetry (CV) was performed for each sample, and the corresponding voltammograms were recorded.

To ensure robustness and reproducibility, CV measurements were repeated six times for each sample and each electrode, resulting in six voltammograms per electrode per sample. With eight samples and five electrodes, the total dataset consisted of 240 voltammograms.

These voltammetric responses were processed using MATLAB to extract key electrochemical features. The extracted variables included:[48]

- $\Delta I = (I_{Ox} - I_{Red})$: Difference between anodic and cathodic peak currents;
- $Slope_{Ox}$: Maximum slope during the oxidation phase;
- $Slope_{Red}$: Maximum slope during the reduction phase;
- Area: Enclosed area under the voltammogram, calculated *via* the trapezoidal method.

Following variable extraction, both supervised and unsupervised data processing techniques were applied to analyze and classify the samples.

Principal Component Analysis (PCA), an unsupervised dimensionality reduction technique, was used to explore sample similarities and identify the variables contributing most significantly to the overall variance.[49] PCA transforms the original variables into new, uncorrelated principal components (PCs), which retain the essential structure of the data and facilitate improved visualization and interpretation.

Discriminant Function Analysis (DFA), a supervised classification technique, was employed in descriptive mode to identify discriminant functions (DFs) that maximize between-class variance while minimizing within-class variance. This approach aids in recognizing patterns and enhancing class separation by projecting data onto dimensions that best represent group differences.

Support Vector Machines (SVMs), developed by Vapnik,[50] were used for supervised classification. This method identifies an optimal hyperplane, known as a support vector (SV), that maximally separates classes. In this study, the "one-against-one" and "one-against-all" multiclass strategies were applied to construct binary classifiers capable of robust classification.[51]

To complement these techniques, Receiver Operating Characteristic (ROC) curve analysis was used as an unsupervised method to assess classification performance and sensitivity. Although typically used for quantitative analysis, ROC was applied here to evaluate the accuracy and reliability of class separation.

In summary, PCA, DFA, and SVMs were employed for qualitative tasks namely dimensionality reduction, feature selection, classification, and visualization of TOB-spiked milk samples. These pattern recognition tools enhanced data interpretation by reducing complexity while preserving key discriminatory information.

3 Results and discussion

3.1 Nanostructures' characterisation

During the fabrication of the TOB MIP sensor, surface morphology and elemental composition of the electrodes were characterized using Fourier-transform infrared spectroscopy (FTIR) and scanning electron microscopy (SEM). The electrode surfaces analyzed included: the bare gold screen-printed electrode (Au-SPE), the modified Au-SPE coated with PANI and AgNPs incorporated into the MIP (Au-SPE/(PANI-AgNPs)/MIP), and the post-extraction version of the MIP-modified electrode (Au-SPE/(PANI-AgNPs)/MIP (Extraction)).

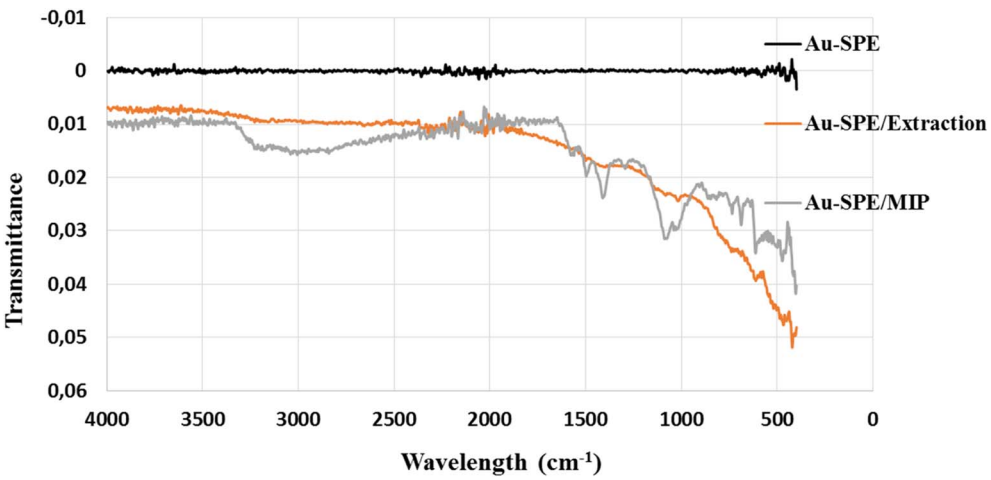

Fig. 3 Fourier transform infrared spectroscopy spectra obtained for bare gold, after molecularly imprinted polymer deposit, and after extraction.

FTIR spectra for the three configurations, bare Au-SPE, Au-SPE/MIP, and Au-SPE/Extraction, are shown in Fig. 3. These spectra provide insight into the chemical composition and molecular interactions at the electrode surface during each stage of modification. The FTIR spectrum of TOB displayed characteristic absorption bands between 1600 and 1300 cm^{-1}, attributable to NH stretching, CH_2 scissoring, and OH bending. A prominent absorption peak around 1000 cm^{-1} was associated with C–O and C–N stretching vibrations. These signature TOB bands were absent in the spectra of both the bare Au-SPE and the extracted MIP electrode (Au-SPE/Extraction), confirming successful TOB incorporation and subsequent removal from the polymer matrix.[52]

Fig. 4 illustrates SEM images of the electrode surfaces at various stages of modification:

Fig. 4A the bare Au-SPE exhibits a homogeneous gold coating with a regular, unmodified morphology.

Fig. 4B after deposition of the PANI-AgNPs and MIP layer, the surface appears more uniform and smoother, indicating successful membrane formation.

Fig. 4C following the extraction of TOB, the electrode surface adopts a porous structure with reduced roughness, likely due to the elution of TOB molecules from the polymer, resulting in the formation of molecular recognition sites.

These FTIR and SEM analyses collectively confirm the structural and chemical changes associated with each modification step and validate the successful imprinting and removal of TOB within the MIP matrix.

3.2 Preparation of TOB imprinted sensors

Electropolymerization provides a simple and effective approach for constructing molecularly imprinted polymer (MIP) films on conductive electrode surfaces. In this study, the process was carried out in a phosphate-buffered saline (PBS) solution (pH 7.2) by applying a potential range from −0.4 V to +0.6 V at a scan rate of 20 mV s^{-1} for 10 cycles. The progression of the film formation was monitored by recording changes in current amplitude across successive cycles. Fig. 5 presents the cyclic voltammograms obtained during the electropolymerization process.

During polymerization, hydrogen bonding interactions occur between the hydroxyl groups (–OH) of TOB and the amine groups ($–NH_2$) of polyaniline (PANI), facilitating the incorporation of TOB into the growing polymer matrix. The inclusion of silver nanoparticles (AgNPs) further enhances this process by increasing the electrode's surface area and enabling the formation of uniformly distributed, spacious binding cavities. These features contribute to the sensor's high sensitivity and selectivity for TOB detection.

3.3 Electrochemical characterizations

Ferri/ferrocyanide ($[Fe(CN)6]^{4-/3-}$) was employed as a redox probe to monitor the entire development of the MIP sensor, providing essential insights into electron transfer between the

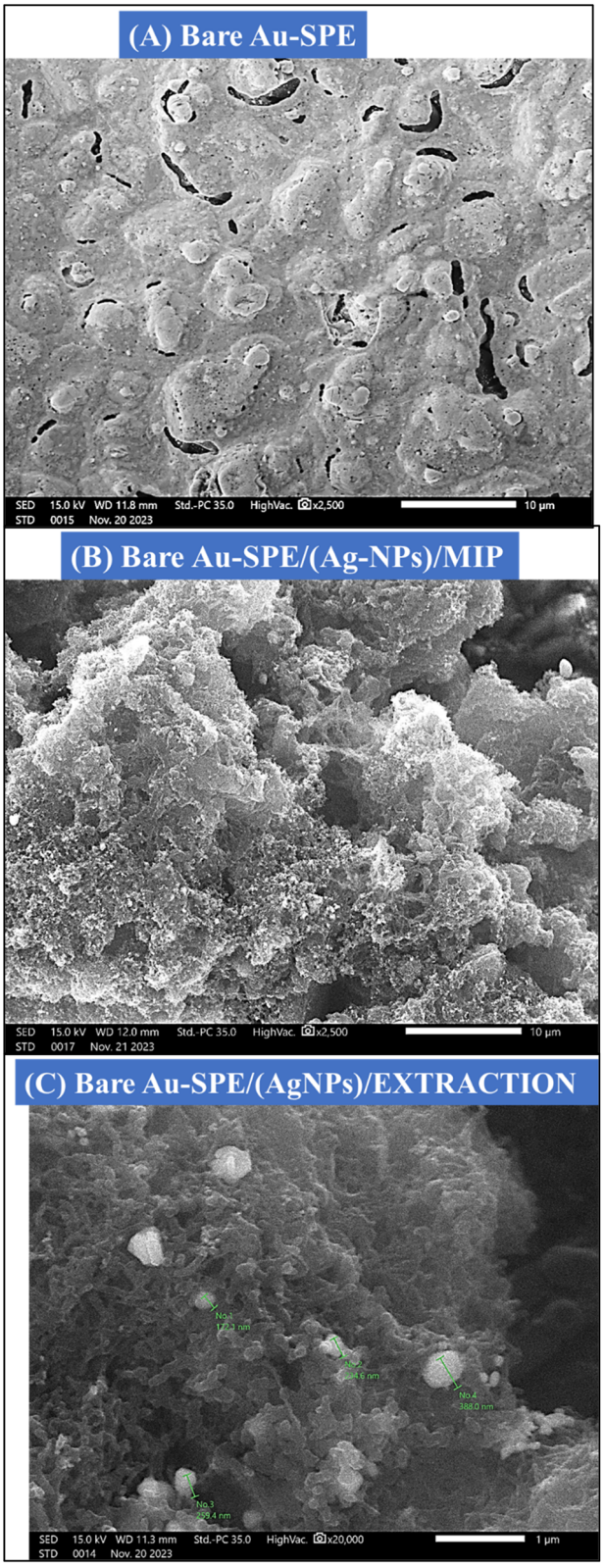

Fig. 4 Scanning electron microscopy images obtained for: (A) Bare gold, (B) after molecularly imprinted polymer deposit, (C) after extraction.

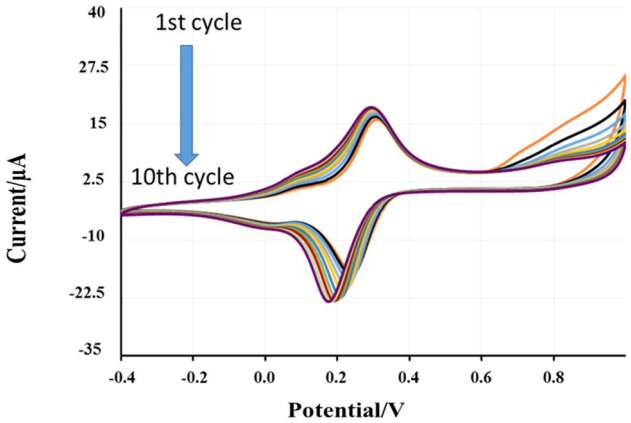

Fig. 5 Cyclic voltammograms of 10 cycles of the electropolymerization of the mixture (silver nanoparticles, polyaniline, and tobramycin).

deposited layer and the electrode surface. Cyclic voltammetry (CV) was used to characterize the electrochemical behavior of the bare Au-SPE, Au-SPE/MIP + AgNPs, and after template extraction. Upon the deposition of the MIP complex on the screen-printed electrode, distinct changes in the shape and amplitude of the electrochemical signals were observed, confirming the successful modification of the gold electrode. Notably, after the analyte extraction process, an increase in signal amplitude was recorded. This observation, supported by the data presented in Fig. 6A, demonstrates the efficient extraction of the analyte from the polymer matrix. The increase in amplitude can be attributed to the creation of vacant sites in the MIP film following TOB removal, which facilitates the electrochemical reaction of the redox probe at the electrode surfaces.

Additionally, EIS is widely recognized as a valuable technique for investigating impedance variations on electrode surfaces during the modification process.[53] The faradaic impedance measurements align well with the CV results, as the diameter of the semicircles observed in the Nyquist diagrams (Fig. 6B) corresponds to variations in the oxidation current peaks indicated by the CV technique (Fig. 6A).

3.4 MIP and NIP responses

The DPV technique is more sensitive than CV and is frequently used in electrochemical detection.[54] The different synthetic concentrations of the TOB solution were used to determine the retention capacity of the developed MIP sensor after template removal. Therefore, to perform the electrochemical and synthetic detection of TOB, 50 μL of a TOB concentration solution was deposited on the working electrode of the MIP sensor. The DPV, and EIS characterization techniques were performed after each retention time (30 min) using PBS containing a 5 mM $[Fe(CN)_6]^{4-/3-}$ solution at room temperature.

The voltammograms presented in Fig. 7A were obtained using differential pulse voltammetry (DPV). A clear decrease in the current peaks of the $[Fe(CN)_6]^{4-/3-}$ signal is observed as TOB concentrations increase. This reduction in current corresponds to the binding of TOB molecules to the imprinted sites on the sensor's surface, which increases with the TOB concentration.

Additionally, a non-imprinted polymer (NIP) test was conducted to validate the sensor responses observed in the MIP test. The NIP test served as a control experiment, in which TOB was omitted during the electropolymerization step. Fig. 7B presents the DPV signals recorded for varying synthetic TOB concentrations using the non-imprinted device. Unlike the MIP sensor, the oxidation current peaks remain nearly unchanged across the TOB concentrations tested. This confirms that the absence of specific recognition cavities in the NIP sensor results in a lack of sensitivity toward TOB, highlighting the specificity of the MIP sensor.

Fig. 8A and B demonstrate the linear relationship between the current peaks and their corresponding concentrations. These figures represent the calibration curves of both MIP and NIP sensors respectively. The plot shows the relative variation of $(I_c - I_0)/I_0$ as a function of the logarithmic concentration of TOB within a linear range of 0.001–60 pg mL^{-1}. As depicted in Fig. 8, the equations expressing the relationship between the relative currents and their corresponding concentrations for MIP and NIP sensors are $y = -0.096 \log(C) - 0.7$, and $y = -0.006 \log(C) - 0.065$, respectively. The LOD is determined using the formula $LOD = 3S_b/m$, where S_b represents the standard deviation of the y-intercept of the regression line, and m is the slope of the calibration curve, based on a signal-to-noise ratio (S/N) of 3.[55–57]

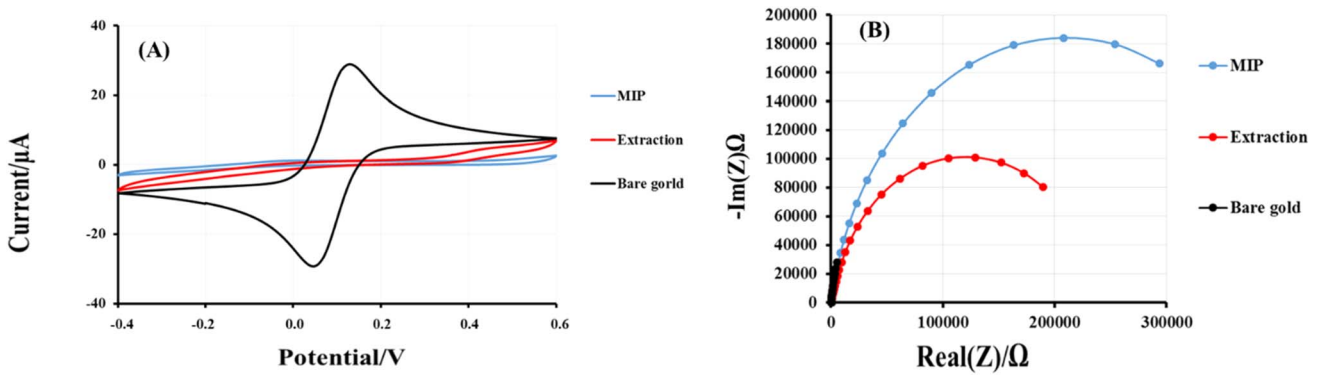

Fig. 6 (A) Cyclic voltammograms of the different stages of molecularly imprinted polymer sensor development, and (B) Nyquist diagrams of different stages in the development of the molecularly imprinted polymer sensor.

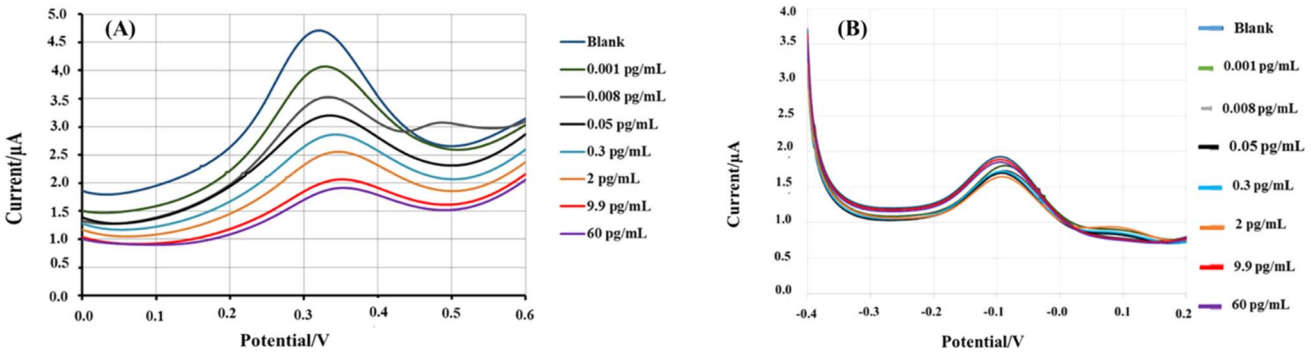

Fig. 7 (A) Cyclic voltammograms of the detection of tobramycin by the molecularly imprinted polymer sensor, and (B) cyclic voltammograms for the detection of tobramycin by the non-imprinted polymer sensor.

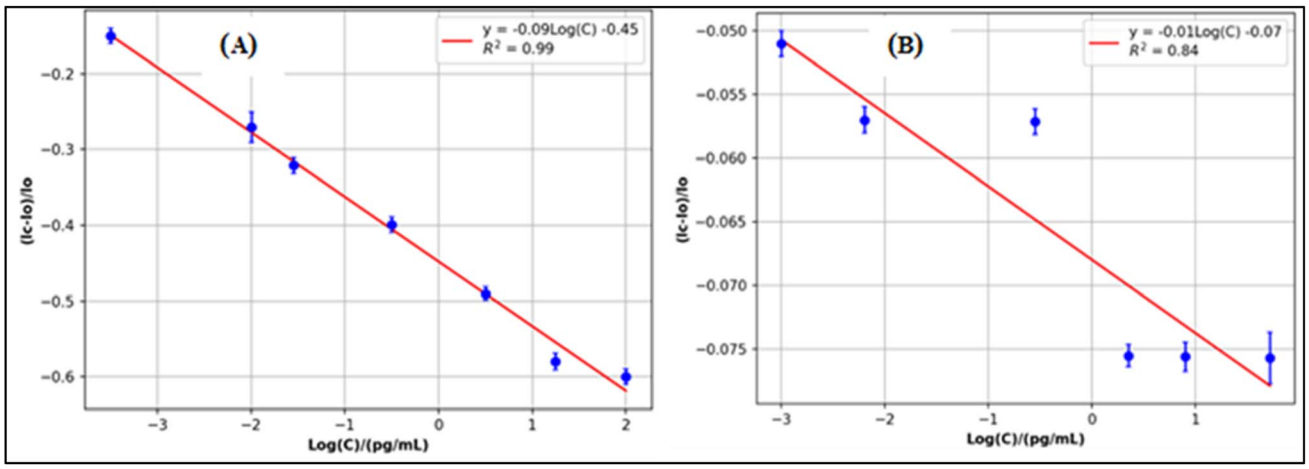

Fig. 8 (A) Differential pulse voltammetry calibration curve of molecularly imprinted polymers sensor, and (B) differential pulse voltammetry calibration curve of non-imprinted polymer sensor.

In the DPV technique, a high coefficient of linearity ($R^2 = 0.99$) is observed across the study range, and the analytical parameters, including LOD and LOQ, are determined to be 1.9 pg mL^{-1}, and 15.8 pg mL^{-1}, respectively.

As per the EIS technique, the charge transfer resistances (R_{ct}) of the MIP sensor increase with an elevation in TOB concentration, as depicted in Fig. 9A. The molecules of TOB are not conductive and are generally not negatively charged, although they may exhibit local positive charges due to their specific

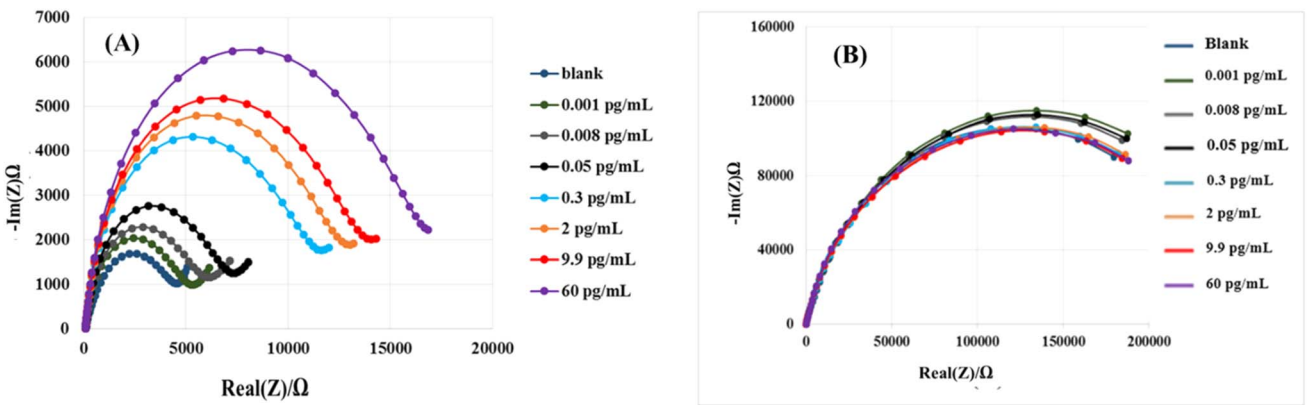

Fig. 9 (A) Nyquist diagrams of tobramycin detection by molecularly imprinted polymers sensor, and (B) Nyquist diagrams of tobramycin detection by the non-imprinted polymer sensor.

functional groups[58] Therefore, the characterization, utilizing a negative redox probe $[Fe(CN)_6]^{4-/3-}$, entailed repulsive interactions between it and the TOB molecules. This might account for the reduction in the observed current peaks and, consequently, the elevation in R_{ct} values with the increasing TOB concentration. These results are consistent with the data shown in Fig. 7A.

Conversely, the NIP sensors exhibited negligible changes in R_{ct}, indicating minimal non-specific interactions between the polymer and TOB (Fig. 9B).

EIS results in the establishment of a logarithmic linear correlation between electrochemical sensor responses and TOB concentration. For each TOB concentration, the value of $(R_c - R_0)/R_0$ was computed. As depicted in Fig. 10A and B, the equations representing the correlation between R_{ct} and their respective concentrations for MIP and NIP are $y = 0.6\log(C) + 1.9$, and $y = 0.006\log(C) - 0.026$, respectively. The EIS findings demonstrate strong consistency with those obtained from DPV. The normalized data for the MIP sensor showed good linearity with R^2 of 0.99 and relationship between TOB concentration and NIP sensor exhibited low linearity coefficient (75%) showing no regular sensitivity. The EIS technique yields LOD and LOQ values of 7.9 pg mL^{-1} and 31.6 pg mL^{-1}, respectively.

Table 2 provides a comparative analysis of experimental data for TOB determination between the relevant MIP sensor and previously reported methods[5,8,59–61] The proposed MIP sensor demonstrates a lower LOD, superior accuracy, and higher sensitivity for detecting TOB traces compared to the reported works. The MIP sensor is very simple for fabrication, logarithmic-linear in a broad range. Therefore, it could be considered a suitable candidate for the future electrochemical sensor of TOB.

3.5 Selectivity, reproducibility, and stability of the MIP sensor

Selectivity is a critical parameter in the design of molecularly imprinted polymer (MIP) sensors, ensuring that the sensor can distinguish the target analyte, in this case, TOB from structurally similar compounds.

To evaluate the selectivity of the MIP sensor, calibration curves were constructed for TOB and four common antibiotic interferents such as gentamicin, tetracycline, ofloxacin, and ciprofloxacin at identical concentrations. As shown in Fig. 11, the slope of each curve was used to calculate the imprinting factor (IF),[62–64] defined as:

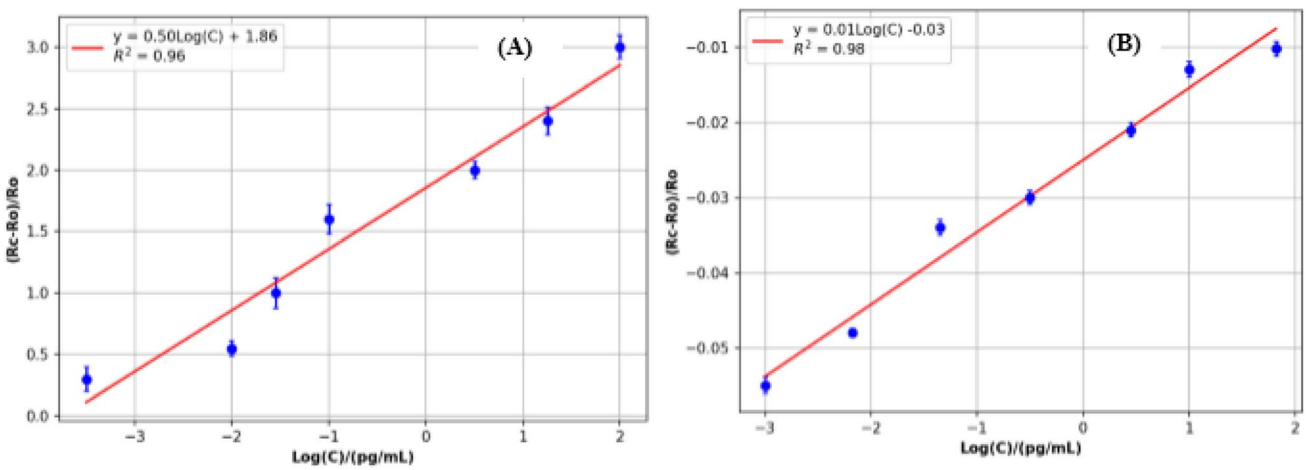

Fig. 10 (A) Calibration curve obtained by electrochemical impedance spectroscopy of the MIP, and (B) calibration curve by electrochemical impedance spectroscopy of the non-imprinted polymer.

Table 2 Comparison of analytical parameters of the proposed molecularly imprinted polymer sensor and reported works for tobramycin detection

Methods	Linear range (pg mL^{-1})	LOD (pg mL^{-1})	LOQ (pg mL^{-1})	Interferences	Real samples	Refs
CRISPR/Cas biosensing, aptamer +++	1.3×10^3–4.6×10^4	3.8×10^2		5	Water	8
HPLC-MS	1.7×10^5–2.5×10^6	5×10^4	1.7×10^5	—	Body fluid	59
ELISA	—	2.5×10^4 5×10^4	—	—	Polystyrene microtiter plates	60
Electrochemical	2.3×10^2–4.6×10^3	65	2.1×10^2	3	Egg and milk	5
Electrochemical	7–70	2	7	3	Egg and milk	61
AuSPE/MIP + AgNPs	**0.001–60**	**1.9**	**15.8**	**4**	**Egg, milk, Turkey, chicken and meat**	**This work**

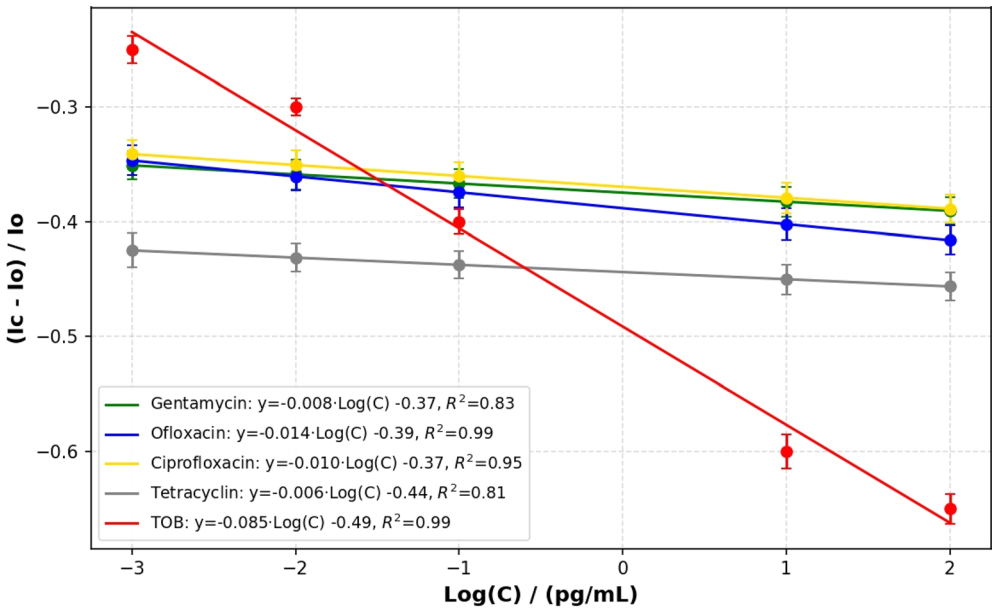

Fig. 11 Sensor responses toward interfering molecules.

IF = SlopeTOB/SlopeINTEREFERENT.

The calculated imprinting factors were of, 10.6, 14, 6, and 8.5 for TOB compared to gentamicin, tetracycline, ofloxacin, and ciprofloxacin, respectively.

These results confirm the high molecular recognition specificity of the MIP sensor for TOB, compared to other structurally related antibiotics.

To assess fabrication reproducibility, three independent MIP sensors were produced under identical conditions. The sensors were tested across the full range of TOB concentrations, and the relative standard deviation (RSD) was found to be ≤ 5%. This low variability indicates high consistency in the manufacturing process.

Repeatability was evaluated by performing three measurements per day over three consecutive days using the same TOB concentration. Between measurements, the MIP sensor was thoroughly rinsed with distilled water. Each cycle included TOB retention, electrochemical analysis, and cleaning steps, with a 40 minutes interval between runs. The sensor exhibited an RSD of less than 5% across all trials, confirming that its responses are stable and repeatable under standard operating conditions.

Moreover, the stability is of great importance for the development of MIP sensors. In this study, it was investigated by monitoring the current response for a TOB solution at regular time interval for a period of 3 months. After this duration, the sensor retained 85% of its initial response. This means that the proposed sensor has acceptable storage stability.

3.6 Recovery in mineral water and milk

To evaluate the practical applicability and reliability of the developed MIP sensor, recovery tests were performed using two real-world samples free of TOB: Ain Soltan mineral water and Milk N°3. Each sample was spiked with four known TOB concentrations: 0.05, 0.3, 2.0, and 9.9 pg mL^{-1}. A fixed aliquot of 50 μL from each spiked solution was applied directly to the MIP sensor's working electrode.

After an appropriate incubation period, the sensor was rinsed with distilled water, and electrochemical detection was conducted using differential pulse voltammetry (DPV). The oxidation current responses obtained were interpreted using the previously established DPV calibration equation: $y = -0.09 \log(C) - 0.45$.

Using this equation, the TOB concentration in each sample was back-calculated. The recovery rates, summarized in Table 3 (mineral water) and Table 4 (milk), ranged from 93.3% to 100%, demonstrating excellent agreement with the spiked concentrations.

These results confirm the sensor's reliability and accuracy for detecting trace levels of TOB in complex sample matrices,

Table 3 Recovery of tobramycin in mineral water (Ain Soltan)

Added concentration (pg mL^{-1})	0.05	0.3	2	9.9
Found concentration (pg mL^{-1})	0.05	0.28	1.9	10
Recovery score (%)	100	93.3	95	100

Table 4 Tobramycin recovery in Chergui milk

Added concentration (pg mL^{-1})	0.05	0.3	2	9.9
Found concentration (pg mL^{-1})	0.05	0.28	1.99	10
Recovery score (%)	100	93.3	99.5	100

validating its potential for real-world applications in both food safety and environmental monitoring.

3.7 Results of application of MIP sensors for TOB detection in real samples

To evaluate the viability of the proposed MIP sensor for real-world applications, it was employed for the electrochemical detection of TOB in various agro-food samples. Sample preparation followed the procedures previously detailed in the experimental section.

The analytical results, summarized in Table 5, demonstrate that several samples including Milk N°1, Milk N°2, Milk N°5, and Milk N°4; beef meat; turkey meat; industrial eggs (non-beldi); and industrial chicken (non-beldi) contained detectable TOB concentrations. These levels were above the sensor's detection limit (1.9 pg mL^{-1}) but remained well below the established maximum residue limits (MRLs) for TOB: 12 μg mL^{-1} in serum and 200 μg mL^{-1} in milk. These findings highlight the sensor's sensitivity and suitability for trace-level detection in complex food matrices.

Conversely, Milk N°3, non-industrial eggs (beldi), and non-industrial chicken (beldi) tested negative for TOB, indicating that the target molecule was absent or present below the detection limit in these samples.

Table 5 Found concentrations of tobramycin in the studied samples

Samples	Concentrations (pg mL^{-1})	Presence
Milk N°1	251	Yes
Milk N°2	12.5	Yes
Milk N°3	0	No
Milk N°4	31.6	Yes
Milk N°5	0.002	Yes
Beldi egg	0	No
Non-beldi egg	0.22	Yes
Beef meat	158	Yes
Turkey meat	20	Yes
Beldi chicken	0	No
Non-beldi chicken	20	Yes

In conclusion, the results confirm the MIP sensor's practicality, sensitivity, and reliability for detecting trace levels of TOB in diverse agro-food products, supporting its application in food safety monitoring and quality control.

3.8 Discrimination of TOB in milk samples by VET

To investigate the presence of TOB residues in milk following ingestion, a qualitative analysis was performed using the voltammetric electronic tongue (VET). This approach aimed to evaluate whether the VET could generate distinguishable electrochemical responses across milk samples spiked with varying TOB concentrations.

Eight milk samples, each containing a different concentration of TOB, were analyzed. The VET system consisted of five metal working electrodes (copper, glassy carbon, platinum, palladium, and gold), which were immersed in the milk samples. Cyclic voltammetry (CV) was conducted over a potential range of −0.2 V to +0.6 V at a scan rate of 50 mV s^{-1}. Each electrode generated a unique cyclic voltammogram depending on its electrochemical interaction with the milk matrix and TOB content.

After each measurement, a strict cleaning protocol was followed to prevent cross-contamination. Electrodes were immersed in piranha solution (30% H_2O_2 : 98% H_2SO_4, 1 : 3 v/v), rinsed with distilled water, polished, and dried to remove all residual contaminants. Piranha solution is frequently used for electrode cleaning because it provides an extremely effective and reliable method for removing organic contaminants, thereby resetting the electrode surface and leaving it very clean and hydrophilic. Its compatibility with various materials, especially noble metals and glass, makes it a "universal" approach. In academic research, it has become a widely recognized standard, ensuring reproducibility and comparability of results across laboratories. Unlike other methods such as plasma or UV-ozone cleaning, it requires no sophisticated equipment, making it accessible. However, its high corrosiveness and significant hazards strongly limit its use in routine applications.

Among the five electrodes, the gold electrode showed the most pronounced and concentration-dependent

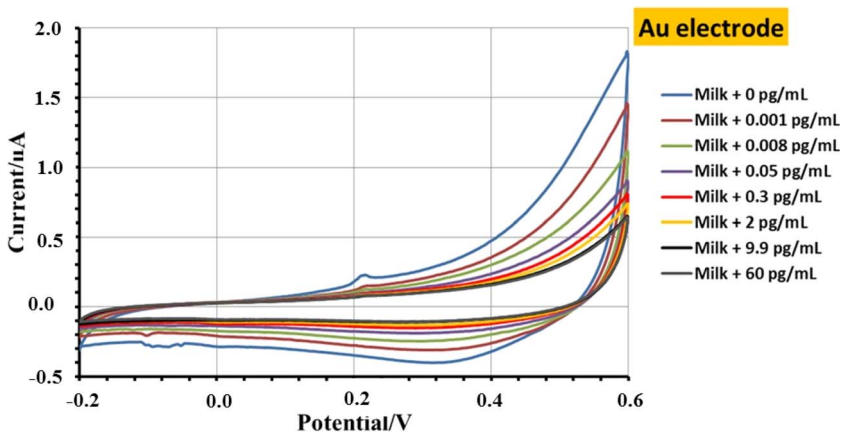

Fig. 12 Mean responses of the voltammetric electronic tongue gold electrode when exposed to eight different milk samples.

electrochemical behavior. Therefore, the average voltammograms from the gold electrode were selected for representation in Fig. 12. The variations in amplitude observed across different samples likely reflect the differences in TOB concentration.

To further evaluate the contribution of each electrode to sample discrimination, a radar plot was generated (Fig. 13), highlighting the distinct electrochemical signatures provided by the multi-electrode array.

The extracted electrochemical features from four electrodes were compiled into a feature matrix and analyzed using MATLAB. This dataset served as the input for pattern recognition algorithms. Principal Component Analysis (PCA), Discriminant Function Analysis (DFA), and Support Vector Machines (SVMs) were applied to improve the classification accuracy and interpretability of the VET's performance.

These findings confirm that the VET system can generate unique, concentration-dependent responses across milk samples and holds strong potential for rapid, qualitative assessment of TOB residues in complex food matrices.

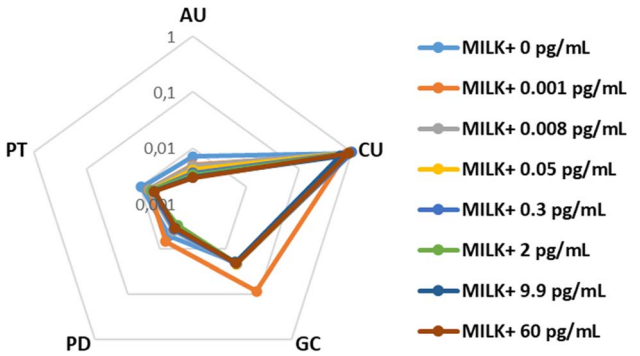

Fig. 13 Radar plots of the voltammetric electronic tongue responses toward the eight different milk samples (expressed as the difference between anodic and cathodic current peaks of cyclic voltammograms).

3.9 Discriminant data analysis models

Following the extraction of key electrochemical features from VET responses, statistical and machine learning techniques were employed to assess the system's discriminative power in differentiating milk samples with varying TOB concentrations.

Principal Component Analysis (PCA) was first applied to reduce the dimensionality of the multivariate dataset and to visualize sample clustering based on electrochemical signatures. As shown in Fig. 14, the first three principal components (PC1, PC2, and PC3) captured a cumulative 94.75% of the total variance in the data, specifically, 50.67% by PC1, 34.89% by PC2, and 9.18% by PC3. The PCA scores plot reveals clear separation between the non-spiked milk sample and those spiked with TOB. Furthermore, distinct groupings were observed among the spiked samples themselves, indicating the VET's capacity to differentiate varying TOB concentrations qualitatively.

To further validate these findings, Discriminant Function Analysis (DFA) was employed. As illustrated in Fig. 15, the DFA score plot confirms effective discrimination between all sample

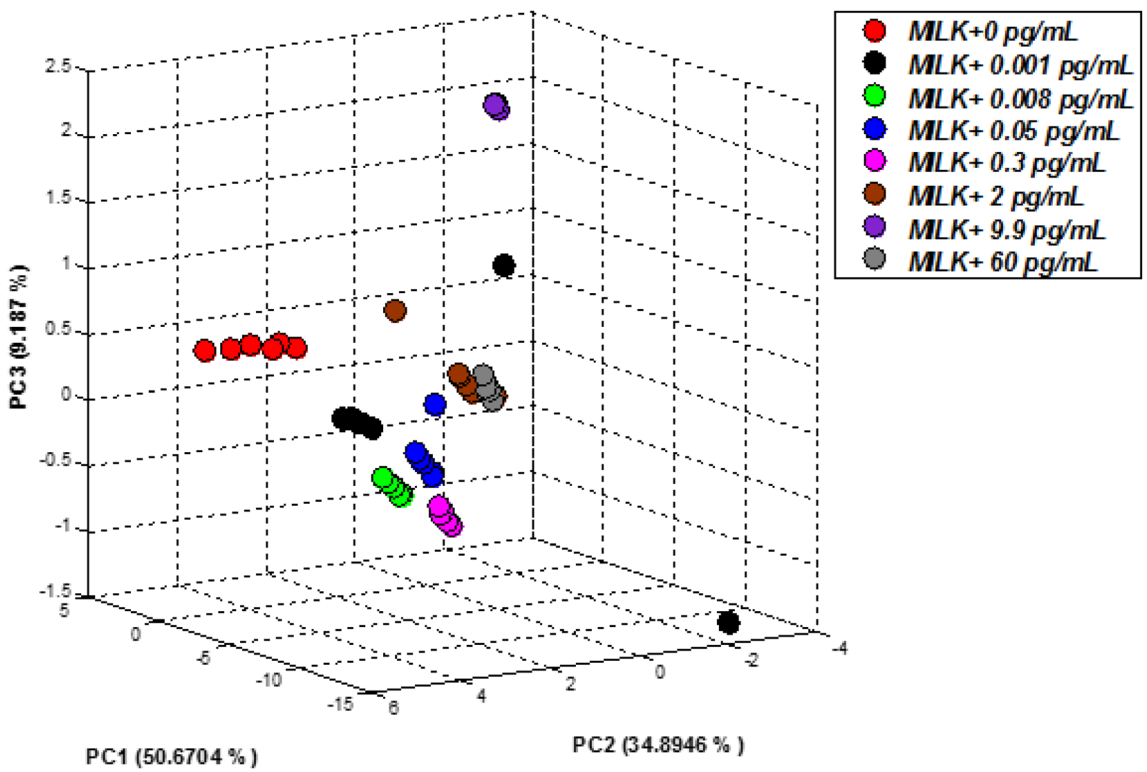

Fig. 14 Principal component analysis plot analysis using Δ*I* and area as features of the voltammetric electronic tongue system responses.

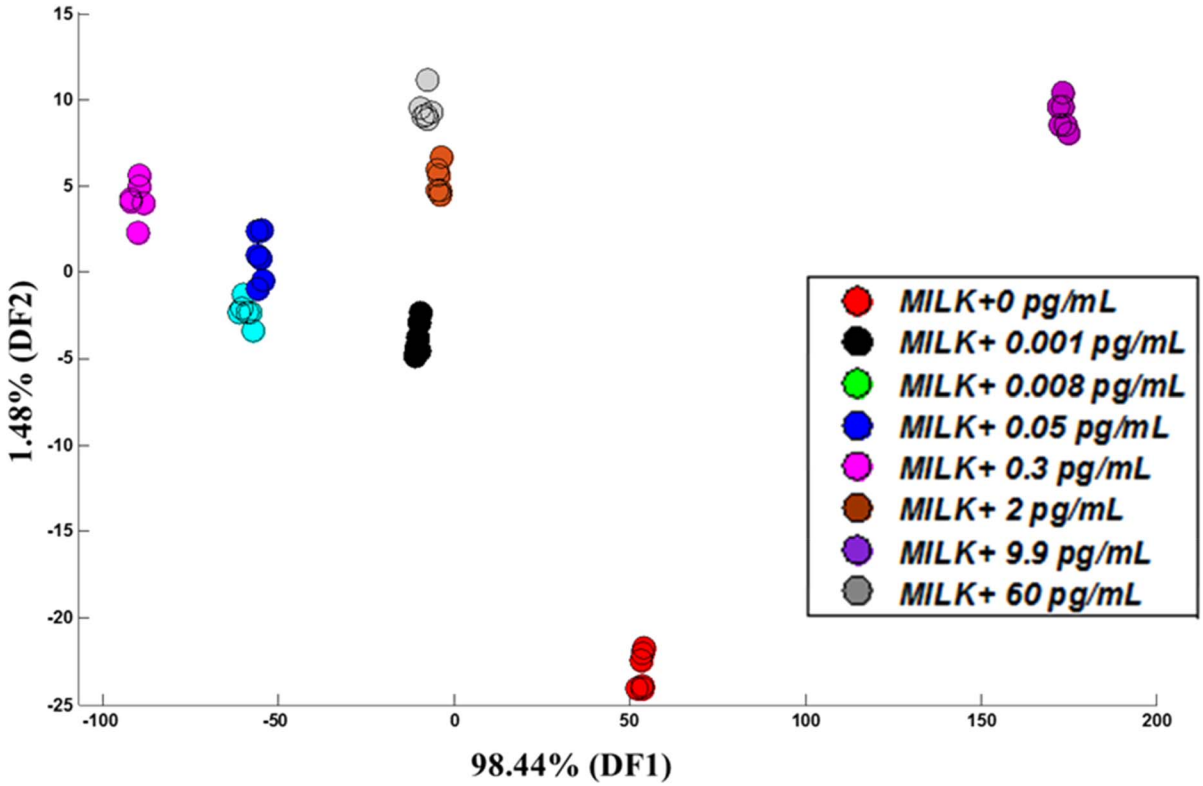

Fig. 15 Discriminant function analysis plot analysis using Δ*I* and Area as features of the voltammetric electronic tongue system responses.

groups, with DF1 accounting for 98.44% and DF2 for 1.48% of the total variance. These results mirror the trends observed in PCA while offering stronger classification performance through supervised learning.

To assess predictive accuracy, a Support Vector Machines (SVMs) classifier was applied to the dataset, with results summarized in the confusion matrix (Table 6). The SVM model achieved an 86.67% classification accuracy across eight distinct milk sample classes: (milk + 0 pg mL^{-1}, milk + 0.001 pg mL^{-1}, milk + 0.008 pg mL^{-1}, milk + 0.05 pg mL^{-1}, milk + 0.3 pg mL^{-1}, milk + 2 pg mL^{-1}, milk + 9.9 pg mL^{-1}, and milk + 60 pg mL^{-1}).

Each sample was correctly classified, aligning with the diagonal of the confusion matrix. The model was validated using a leave-one-out cross-validation method to reduce bias and mitigate the effects of a limited dataset, which can lead to overfitting.

While overfitting is a known limitation in models trained on small datasets, previous work, such as that of Smulko *et al.* (2015)[65] has addressed this using least squares SVMs and larger datasets to improve generalizability. Recent enhancements in SVM methodologies continue to strengthen resistance to overfitting and improve model robustness.[66–69]

In summary, PCA and DFA confirmed the VET's ability to differentiate milk samples based on TOB content, with DFA showing superior classification precision by consistently maintaining the relative spatial topology of sample groups. These findings further establish the VET system's effectiveness as a qualitative tool for TOB detection in complex biological matrices.

Table 6 Support vector machines results for the classification of 24 milk samples regarding different concentration of tobramycin by using the VET system with a success rate of 86.67%

Actual	Class 1	2	0	0	0	0	0	0	0
	Class 2	0	1		0	0	0	1	0
	Class 3	0	0	1	0	0	0	0	0
	Class 4	0	0	1	0	0	0	0	0
	Class 5	0	0	0	0	4	0	0	0
	Class 6	0	0	0	0	0	1	0	0
	Class 7	0	0	0	0	0	0	3	0
	Class 8	0	0	0	0	0	0	0	1
		Class 1	Class 2	Class 3	Class 4	Class 5	Class 6	Class 7	Class 8
	Predicted								

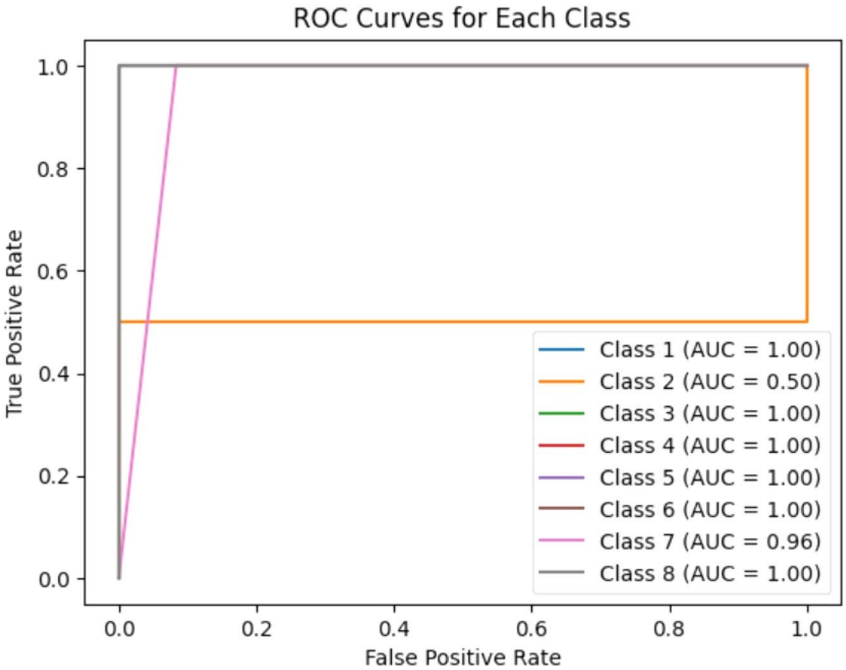

Fig. 16 Receiver operating characteristic curve displaying data points for eight different milk samples with data collected from the voltammetric electronic tongue.

3.10 Receiver operating characteristic (ROC) curves

The Receiver Operating Characteristic (ROC) curve is a graphical tool used to evaluate the classification performance of predictive models. It plots the true positive rate (sensitivity) against the false positive rate (1-specificity) for each class. In this study, the ROC analysis was applied to assess the performance of the VET-based classification model across eight TOB concentration classes: Class 1: 0 pg mL^{-1}; Class 2: 0.001 pg mL^{-1}; Class 3: 0.008 pg mL^{-1}; Class 4: 0.05 pg mL^{-1}; Class 5: 0.3 pg mL^{-1}; Class 6: 2 pg mL^{-1}; Class 7: 9.9 pg mL^{-1}; Class 8: 60 pg mL^{-1}; As shown in Fig. 16, the ROC curves illustrate the model's ability to discriminate between these classes. The Area Under the Curve (AUC) serves as a quantitative metric of model accuracy for each class.

Perfect classification (AUC = 1.00) was achieved for Classes 1, 3, 4, 5, 6, and 8, indicating that the model successfully distinguished these TOB levels without misclassification.

Class 7 achieved an AUC of 0.96, reflecting strong but not flawless performance.

Class 2, however, displayed an AUC of 0.50, suggesting performance equivalent to random guessing, and indicating that the model struggled to distinguish this concentration level from the others.

Curves that sharply rise toward the upper left corner of the ROC plot reflect high classification accuracy. In contrast, curves that align closely with the diagonal (as seen for Class 2) indicate poor discrimination capability.

Overall, the ROC analysis confirms that the model demonstrates excellent classification performance for most TOB concentration classes, with the notable exception of Class 2. This highlights a need for further refinement potentially through enhanced feature selection, additional training data, or class balancing to improve accuracy at the lowest concentration levels.

4 Conclusion

This study successfully developed an electrochemical MIP sensor that integrates conductive polymers and metallic nanoparticles, resulting in a sensitive, selective, and cost-effective tool for detecting TOB in food samples. When applied to real-world matrices like milk, the sensor paired with a VET system demonstrated strong quantitative and qualitative analytical performance. A detection limit of 1.9 pg mL^{-1} and a limit of quantification (LOQ) of 15.8 pg mL^{-1} were achieved over the working range. The wide dynamic range (0.001–60 pg mL^{-1}), clear logarithmic-linear response, and minimal sample preparation requirements make it a practical alternative to more complex laboratory-based methods.

Compared to conventional techniques, the proposed approach offers several distinct advantages: affordability, ease of use, high sensitivity, and portability. These qualities position it as a strong candidate for routine screening of antibiotic residues, particularly in environments where resources or technical infrastructure are limited.

Looking ahead, this platform has the potential for significant expansion. Future research could explore the sensor's adaptability to a broader range of antibiotics and other contaminants, including pesticides, hormones, or mycotoxins. Additionally, integration with wireless or smartphone-based readout systems could enable real-time, on-site monitoring, an advancement that would be particularly beneficial in supply chain management and field testing.

From a regulatory perspective, the sensor aligns well with global efforts to enforce stricter food safety standards. Its rapid response time and minimal operational requirements can support more frequent and decentralized testing, ultimately contributing to better public health outcomes. Furthermore, its design principles could inform the development of next-generation electrochemical sensors for clinical, environmental, or pharmaceutical applications.

In sum, this study not only presents a robust solution for current challenges in food safety monitoring but also opens the door to broader innovations in electrochemical sensing technologies, with promising implications for research, industry, and public health.

Author contributions

Conceptualization, B. B. and N. E.; measurement methodology, M. W; validation, M. W; resources, N. E.; writing—original draft preparation, M. W.; writing—review and editing, B. B. and N. E.; supervision, B. B.; project administration, N. E.; funding acquisition, N. E. All authors have read and agreed to the published version of the manuscript.

Conflicts of interest

The authors declare no conflict of interest.

Data availability

The data that support the findings of this study are available upon your request.

Acknowledgements

The authors acknowledge the support provided by Moulay Ismaïl University of Meknes, and H2020-MSCA-RISE-2020 project. Authors gratefully acknowledge Moulay Ismaïl University of Meknes for financial support of the project "Research support, Project UMI-2018". This work was also supported by H2020-MSCA-RISE-2020 project, grant agreement ID: 101007653: "Non-invasive volatiles test for canine leishmaniasis diagnosis".

References

1 N. Krithiga, V. S. Vasantha and A. Jayachitra, Highly sensitive detection of carcinoembryonic antigen *via* an electrochemical platform fabricated by CCLP-gold nanocomposite, *J. Immunol. Methods*, 2025, **539**, 113848.

2 R. Islam, H. T. Le Luu and S. Kuss, Electrochemical approaches and advances towards the detection of drug resistance, *J. Electrochem. Soc.*, 2020, **167**(4), 045501.

3 A. Joshi and K. H. Kim, Recent advances in nanomaterial-based electrochemical detection of antibiotics: Challenges and future perspectives, *Biosens. Bioelectron.*, 2020, **153**, 112046.

4 J. He, N. Li, D. Zhang, G. Zheng, H. Zhang, K. Yu and J. Jiang, Real-time monitoring of ciprofloxacin degradation in an electro-Fenton-like system using electrochemical-mass spectrometry, *Environ. Sci.:Water Res. Technol.*, 2020, **6**(1), 181–188.

5 V. K. Gupta, M. L. Yola, N. Özaltın, N. Atar, Z. Üstündağ and L. Uzun, Molecular imprinted polypyrrole modified glassy carbon electrode for the determination of Tobramycin, *Electrochim. Acta*, 2013, **112**, 37–43.

6 R. Oertel, V. Neumeister and W. Kirch, Hydrophilic interaction chromatography combined with tandem-mass spectrometry to determine six aminoglycosides in serum, *J. Chromatogr. A*, 2004, **1058**(1–2), 197–201.

7 T. Da Silva Medeiros, E. C. Pinto, L. M. Cabral and V. P. T. de Sousa, A review of detectors used in analytical approaches for drug substance, its impurities, and in pharmaceutical formulation, *Microchem. J.*, 2021, **160**, 105658.

8 Z. Deng, J. Hu, R. Liu and Y. Lv, Elemental Probe-Based CRISPR/Cas12a Biosensing for Sensitive Tobramycin Detection, *At. Spectrosc.*, 2022, **43**, 201–206.

9 J. G. Hardman and L. E. Limbird *Pharmacological Basis of Therapeutics*. Neurotransmission 2001.

10 F. Nasri, M. Hosseini, S. M. Taghdisi, M. R. Ganjali and M. Ramezani, Design and application of an ultrasensitive and selective tobramycin electrochemiluminescence aptasensor using MXene/Ni/Sm-LDH-based nanocomposite, *Microchim. Acta*, 2024, **191**(9), 506.

11 A. Moga, M. Vergara-Barberán, M. J. Lerma-García, E. J. Carrasco-Correa, J. M. Herrero-Martínez and E. F. Simó-Alfonso, Determination of antibiotics in meat samples using analytical methodologies: A review, *Compr. Rev. Food Sci. Food Saf.*, 2021, **20**(2), 1681–1716.

12 M. A. Rosasco, S. L. Bonafede, S. N. Faudone and A. I. Segall, Compatibility study of Tobramycin and pharmaceutical excipients using differential scanning calorimetry, FTIR, DRX, and HPLC, *J. Therm. Anal. Calorim.*, 2018, **134**, 1929–1941.

13 J. B. Arsand, L. Jank, M. T. Martins, R. B. Hoff, F. Barreto, T. M. Pizzolato and C. Sirtori, Determination of aminoglycoside residues in milk and muscle based on a simple and fast extraction procedure followed by liquid chromatography coupled to tandem mass spectrometry and time of flight mass spectrometry, *Talanta*, 2016, **154**, 38–45.

14 W. C. Yang, A. M. Yu and H. Y. Chen, Applications of a copper microparticle-modified carbon fiber microdisk array electrode for the simultaneous determination of aminoglycoside antibiotics by capillary electrophoresis, *J. Chromatogr. A*, 2001, **905**(1–2), 309–318.

15 P. Tavakoli, S. M. Taghdisi, P. Maghami and K. Abnous, A novel aptasensor for colorimetric monitoring of Tobramycin: Strategy of enzyme-like activity of AuNPs controlled by three-way junction DNA pockets, *Spectrochim. Acta, Part A*, 2022, **267**, 120626.

16 Y. Zhao, Q. Chen, Y. Liu, B. Jiang, R. Yuan and Y. Xiang, A sensitive tobramycin electrochemical aptasensor based on

multiple signal amplification cascades, *Bioelectrochemistry*, 2024, **160**, 108797.

17 R. Monošík, P. Magdolen, M. Streďanský and E. Šturdík, Monitoring of monosaccharides, oligosaccharides, ethanol, and glycerol during wort fermentation by biosensors, HPLC, and spectrophotometry, *Food Chem.*, 2013, **138**(1), 220–226.

18 S. Motia, B. Bouchikhi, E. Llobet and N. El Bari, Synthesis and characterization of a highly sensitive and selective electrochemical sensor based on molecularly imprinted polymer with gold nanoparticles modified screen-printed electrode for glycerol determination in wastewater, *Talanta*, 2020, **216**, 120953.

19 Y. Ou, X. Jin, J. Fang, Y. Tian and N. Zhou, Multi-cycle signal-amplified colorimetric detection of Tobramycin based on dual-strand displacement and three-way DNA junction, *Microchem. J.*, 2020, **156**, 104823.

20 A. Ait Lahcen, S. Ait Errayess and A. Amine, Voltammetric determination of sulfonamides using paste electrodes based on various carbon nanomaterials, *Microchim. Acta*, 2016, **183**, 2169–2176.

21 T. Wang, S. Xu, L. Liu, *et al.*, A highly stable voltammetric sensor for trace ofloxacin determination coupling molecularly imprinting film with AuNP and UiO-66 MOF dual-encapsulated black phosphorus nanosheets, *Mater. Today Chem.*, 2025, **43**, 102468.

22 A. G. Ayankojo, J. Reut, V. Ciocan, A. Öpik and V. Syritski, Molecularly imprinted polymer-based sensor for electrochemical detection of erythromycin, *Talanta*, 2020, **209**, 120502.

23 P. S. Sharma, A. Pietrzyk-Le, F. D'souza and W. Kutner, Electrochemically synthesized polymers in molecular imprinting for chemical sensing, *Anal. Bioanal. Chem.*, 2012, **402**, 3177–3204.

24 G. Lai, H. Zhang, J. Yong and A. Yu, In situ deposition of gold nanoparticles on polydopamine functionalized silica nanosphere for ultrasensitive nonenzymatic electrochemical immunoassay, *Biosens. Bioelectron.*, 2013, **47**, 178–183.

25 D. Martín-Yerga, A. Pérez-Junquera, M. B. González-García, J. V. Perales-Rondon, A. Heras, A. Colina and P. Fanjul-Bolado, Quantitative Raman spectroelectrochemistry using silver screen-printed electrodes, *Electrochim. Acta*, 2018, **264**, 183–190.

26 N. V. Skorodumova and S. I. Simak, Stability of gold nanowires at large Au-Au separations, *Phys. Rev. B*, 2003, **67**(12), 121404.

27 K. Zhao, X. Ma, M. Wang, Z. Qu, H. Chen, B. He and B. Zhang, Electrochemical aptamer sensor based on AgNPs@PDANSs and "sandwich" structure guidance for the detection of Tobramycin in water samples, *Anal. Methods*, 2024, **16**(33), 5665–5675.

28 Y. Zhang, B. Li, X. Wei, Q. Gu, M. Chen, J. Zhang and Q. Wu, Amplified electrochemical antibiotic aptasensing based on electrochemically deposited AuNPs coordinated with PEI-functionalized Fe-based metal-organic framework, *Microchim. Acta*, 2021, **188**, 1–11.

29 D. N. da Silva and A. C. Pereira, Relevant aspects in the development of electrochemical aptasensors for the determination of antibiotics—A review, *Electrochem*, 2023, **4**(4), 553–567.

30 E. Fu, K. Khederlou, N. Lefevre, S. A. Ramsey, M. L. Johnston and L. Wentland, Progress on electrochemical sensing of pharmaceutical drugs in complex biofluids, *Chemosensors*, 2023, **11**(8), 467.

31 S. Wang, Z. Li, F. Duan, B. Hu, L. He, M. Wang and Z. Zhang, Bimetallic cerium/copper organic framework-derived cerium and copper oxides embedded by mesoporous carbon: Label-free aptasensor for ultrasensitive Tobramycin detection, *Anal. Chim. Acta*, 2019, **1047**, 150–162.

32 J. J. García-Guzmán, C. Pérez-Ràfols, M. Cuartero and G. A. Crespo, Microneedle-based electrochemical (bio)-sensing: Towards decentralized and continuous health status monitoring, *Trends Anal. Chem.*, 2021, **135**, 116148.

33 M. Negahdary, Electrochemical aptasensors based on the gold nanostructures, *Talanta*, 2020, **216**, 120999.

34 X. Liu, Y. Jiang, J. Luo, X. Guo, Y. Ying, Y. Wen and Y. Wu, A SnO_2/Bi_2S_3-based photoelectrochemical aptasensor for sensitive detection of Tobramycin in milk, *Food Chem.*, 2021, **344**, 128716.

35 D. Ha, Q. Sun, K. Su, H. Wan, H. Li, N. Xu and P. Wang, Recent achievements in electronic tongue and bioelectronic tongue as taste sensors, *Sens. Actuators, B*, 2015, **207**, 1136–1146.

36 T. P. Huynh and W. Kutner, Molecularly imprinted polymers as recognition materials for electronic tongues, *Biosens. Bioelectron.*, 2015, **74**, 856–864.

37 C. Pérez-Ràfols, N. Serrano, J. M. Díaz-Cruz, C. Ariño and M. Esteban, A screen-printed voltammetric electronic tongue for the analysis of complex mixtures of metal ions, *Sens. Actuators, B*, 2017, **250**, 393–401.

38 A. Diouf, Y. Aghoutane, H. Burhan, F. Sen, B. Bouchikhi and N. El Bari, Tramadol sensing in non-invasive biological fluids using a voltammetric electronic tongue and an electrochemical sensor based on biomimetic recognition, *Int. J. Pharm.*, 2021, **593**, 120114.

39 Y. Vlasov, A. Legin, A. Rudnitskaya, C. Di Natale and A. D'amico, Nonspecific sensor arrays ("electronic tongue") for chemical analysis of liquids (IUPAC Technical Report), *Pure Appl. Chem.*, 2005, **77**(11), 1965–1983.

40 Z. Zhang, N. Zhu, Y. Zou, X. Wu, G. Qu and J. Shi, A novel, enzyme-linked immunosorbent assay based on the catalysis of AuNCs@BSA-induced signal amplification for the detection of dibutyl phthalate, *Talanta*, 2018, **179**, 64–69.

41 M. Ayad, G. El-Hefnawy and S. Zaghlol, Facile synthesis of polyaniline nanoparticles; its adsorption behavior, *Chem. Eng. J.*, 2013, **217**, 460–465.

42 F. X. Perrin *Synthèse de polyaniline en systèmes micellaires: application à la protection des métaux. Theses.fr*, 2014.

43 C. Wang, X. Yin, L. Zhang, N. Ye and Y. Xiang, Synthesis of polyadenine-aptamer-stabilized gold nanoclusters and application to the detection of tobramycin in real samples based on their peroxidase-like activity, *Food Chem.*, 2025, 143194.

44 Q. Ma, Y. Wang, J. Jia and Y. Xiang, Colorimetric aptasensors for determination of Tobramycin in milk and chicken eggs based on DNA and gold nanoparticles, *Food Chem.*, 2018, **249**, 98–103.
45 L. Qiao, Y. Zhu, T. Zeng, Y. Zhang, M. Zhang, K. Song and C. Zhang, Turn-off" photoelectrochemical aptasensor based on g-C_3N_4/WC/WO_3 composites for Tobramycin detection, *Food Chem.*, 2023, **403**, 134287.
46 B. D. Abera, I. Ortiz-Gómez, B. Shkodra, F. J. Romero, G. Cantarella, L. Petti and A. Rivadeneyra, Laser-induced graphene electrodes modified with a molecularly imprinted polymer for detection of tetracycline in milk and meat, *Sensors*, 2021, **22**(1), 269.
47 Z. Q. Jiang, H. C. Zhang, X. Y. Zhang and J. P. Wang, Determination of tetracyclines in milk with a molecularly imprinted polymer-based microtiter chemiluminescence sensor, *Anal. Lett.*, 2019, **52**(8), 1315–1327.
48 Z. Haddi *Conception et développement d'un système multicapteurs en gaz et en liquide pour la sécurité alimentaire. Thèse de doctorat*, Université Claude Bernard-Lyon I et Université Moulay Ismaïl, 2013.
49 I. T. Jolliffe and J. Cadima, Principal Component analysis: A review and recent developments, *Philos. Trans. R. Soc., A*, 2016, **374**(2065), 20150202.
50 V. Vapnik, The support vector method of function estimation, in *Nonlinear Modeling: Advanced Black-Box Techniques*, Springer US, Boston, MA, 1998, pp. 55–85.
51 N. El Barbri, E. Llobet, N. El Bari, X. Correig and B. Bouchikhi, Electronic nose based on metal oxide semiconductor sensors as an alternative technique for the spoilage classification of red meat, *Sensors*, 2008, **8**(1), 142–156.
52 P. Chetoni, S. Burgalassi, D. Monti, S. Tampucci, V. Tullio, A. M. Cuffini and R. Cavalli, Solid lipid nanoparticles as a promising tool for intraocular Tobramycin delivery: Pharmacokinetic studies on rabbits, *Eur. J. Pharm. Biopharm.*, 2016, **109**, 214–223.
53 Y. Sun, H. Yang, X. Yu, H. Meng and X. Xu, A novel non-enzymatic amperometric glucose sensor based on a hollow Pt–Ni alloy nanotube array electrode with enhanced sensitivity, *RSC Adv.*, 2015, **5**(86), 70387–70394.
54 A. Diouf, N. El Bari and B. Bouchikhi, A novel electrochemical sensor based on ion-imprinted polymer and gold nanomaterials for nitrite ion analysis in exhaled breath condensate, *Talanta*, 2020, **209**, 120577.
55 S. Motia, I. A. Tudor, P. A. Ribeiro, M. Raposo, B. Bouchikhi and N. El Bari, Electrochemical sensor based on molecularly imprinted polymer for sensitive triclosan detection in wastewater and mineral water, *Sci. Total Environ.*, 2019, **664**, 647–658.
56 Y. Aghoutane, A. Diouf, L. Österlund, B. Bouchikhi and N. El Bari, Development of a molecularly imprinted polymer electrochemical sensor and its application for sensitive detection and determination of malathion in olive fruits and oils, *Bioelectrochemistry*, 2020, **132**, 107404.
57 S. Motia, I. A. Tudor, L. M. Popescu, R. M. Piticescu, B. Bouchikhi and N. El Bari, Development of a novel electrochemical sensor based on electropolymerized molecularly imprinted polymer for selective detection of sodium lauryl sulfate in environmental waters and cosmetic products, *J. Electroanal. Chem.*, 2018, **823**, 553–562.
58 W. Zhou, Z. Jia, P. Xiong, J. Yan, M. Li, Y. Cheng and Y. Zheng, Novel pH-responsive Tobramycin-embedded micelles in nanostructured multilayer-coatings of chitosan/heparin with efficient and sustained antibacterial properties, *Mater. Sci. Eng., C*, 2018, **90**, 693–705.
59 F. Valentini, P. L. Buldini, E. Landi, *et al.*, HPLC determination of tobramycin in a simulated body fluid, *Microchem. J.*, 2008, **90**, 113–117.
60 S. Sachetelli, C. Beaulac and J. Lagacé, Aminoglycoside detection using a universal ELISA binding procedure onto polystyrene microtiter plates in comparison with HPLC analysis and microbiological agar-diffusion assay, *Biochim. Biophys. Acta, Gen. Subj.*, 1998, **1379**, 35–41.
61 M. L. Yola, L. Uzun, N. Özaltın and A. Denizli, Development of molecular imprinted nanosensor for determination of Tobramycin in pharmaceuticals and foods, *Talanta*, 2014, **120**, 318–324.
62 B. Deiminiat, G. H. Rounaghi and M. H. Arbab-Zavar, Development of a new electrochemical imprinted sensor based on poly-pyrrole, sol–gel and multiwall carbon nanotubes for determination of tramadol, *Sens. Actuators, B*, 2017, **238**, 651–659.
63 A. S. Nair and M. P. Sooraj, Molecular imprinted polymer-wrapped AgNPs-decorated acid-functionalized graphene oxide as a potent electrochemical sensor for ibuprofen, *J. Mater. Sci.*, 2020, **55**(8), 3700–3711.
64 W. J. Peveler, M. Yazdani and V. M. Rotello, Selectivity and specificity: Pros and cons in sensing, *ACS Sens.*, 2016, **1**(11), 1282–1285.
65 J. M. Smulko, R. Ionescu, C. G. Granqvist and L. B. Kish, Determination of gas mixture components using fluctuation enhanced sensing and the LS-SVM regression algorithm, *Metrol. Meas. Syst.*, 2015, **22**(3), 341–350.
66 L. Zhou, W. Zhang and H. Wang, Sparse SVM with adaptive LpLp-norm regularization for high-dimensional small-sample learning, *IEEE Trans. Neural Netw. Learn. Syst.*, 2024, **35**(2), 1124–1137.
67 S. Park and K. Jung, Meta-learning for multi-kernel SVM optimization: A bias-variance tradeoff perspective, *Expert Syst. Appl.*, 2024, **238**(Part A), 121801.
68 T. Chen, Y. Li and Q. Zhang, Privacy-preserving federated SVMs for distributed small-data applications, *Pattern Recognit.*, 2025, **151**, 110352.
69 R. Liu, X. Gao and J. S. Yang, A hybrid reweighting approach for imbalanced small datasets, *Neural Process. Lett.*, 2025, **57**(1), 1–23.